DOI: 10.1002/ejic.201000315

Mono- and Dinuclear Ni^{II} and Co^{II} Complexes that Feature Chelating Guanidine Ligands: Structural Characteristics and Molecular Magnetism

Pascal Roquette,[a] Carolin König,[a] Olaf Hübner,[a] Arne Wagner,[a] Elisabeth Kaifer,[a] Markus Enders,[a] and Hans-Jörg Himmel*[a]

Keywords: Guanidines / Nickel / Cobalt / Structure elucidation / Molecular magnetism

Several new mono- and dinuclear complexes of Co^{II} and Ni^{II} with chelating guanidine ligands were synthesized. The molecular structures for most of the complexes in the crystalline state were derived from single-crystal X-ray diffraction, and some characteristic structural details are discussed. The molecular magnetism was further studied by superconducting quantum interference device (SQUID) measurements. In addition to the experiments, quantum chemical calculations were carried out. Finally, the paramagnetic NMR spectra for one of the complexes are discussed, which shows that $^1J_{C,H}$ correlation experiments are possible.

Introduction

Neutral guanidine ligands have been used intensively in the past in coordination chemistry.[1,2] They represent not only excellent σ-donor, but also π-donor ligands. Several synthetic methods were established to allow a sophisticated and directed ligand design.[3] Herein we report on the synthesis and characterization of some mono- and dinuclear Co^{II} and Ni^{II} complexes that feature chelating guanidine ligands with aromatic backbones. Scheme 1 includes the Lewis structures of a selection of ligands applied for the synthesis of mononuclear complexes. A number of late- and post-transition-metal complexes of the ligand 1,2-bis(tetramethylguanidino)benzene (btmgb)[4] are now known.[5,6] In a previous work we analyzed the magnetism and electronic structure in mononuclear Ni^{II} complexes of this and other chelating guanidine ligands.[7] A significant zero-field splitting parameter *D* was found in these studies with consequences for the temperature dependence of the magnetic susceptibility below approximately 25 K. Sundermeyer et al. established 2,8-bis(tetramethylguanidino)naphthalene (btmgn) as a kinetically active proton sponge.[8] Work by our group showed this ligand to coordinate to late- and post-transition metal ions;[9] however, the metal ion in these complexes generally is heavily displaced from the aromatic plane of the ligand, with consequences for the (catalytic) reactivity. Hence, for example, the Pt^{II} ions in [(btmgn)-$PtCl_2$] are displaced by 133.1 pm from the "best plane" of the naphthyl backbone.[9] In some cases, coordination leads to a considerable distortion of the aromatic backbone. Other chelating guanidine ligands, in which the two amino N atoms of each guanidino group are connected by an ethylene (C_2H_4) bridge, were already previously described.[10,11] This concept was further extended to C_2H_2 bridges, thus realizing imidazolin-2-imines[12] and increasing the σ-donor character of the ligands, which were later shown to be active in catalytic reactions.[13,14] In this work, we used the ligand 1,2-bis(*N*,*N*′-dimethylethyleneguanidino)benzene (bdmegb), the synthesis of which was described previously,[15] for the preparation of mononuclear Co^{II} and Ni^{II} complexes. Due to fast electron relaxation of high-spin

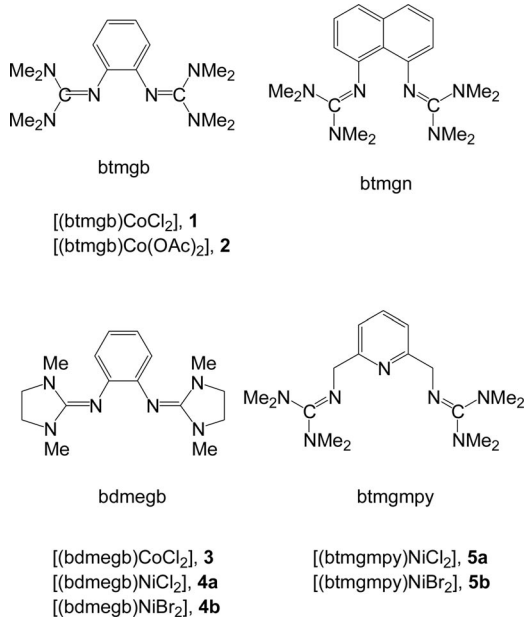

Scheme 1.

[a] Anorganisch-Chemisches Institut,
Ruprecht-Karls-Universität Heidelberg,
Im Neuenheimer Feld 270, 69120 Heidelberg, Germany
Fax: +49-6221-545707
E-mail: hans-jorg.himmel@aci.uni-heidelberg.de

Supporting information for this article is available on the WWW under http://dx.doi.org/10.1002/ejic.201000315.

Co^{II}, the complex [(bdmegb)$CoCl_2$] is ideally suited for paramagnetic NMR spectroscopic studies, including $^1J_{C,H}$ correlation experiments. Finally, the ligand 2,6-bis(tetramethylguanidinomethyl)pyridine (btmgmpy) offers a third coordination site and is thus expected to coordinate differently.[16]

Recently, we introduced aromatic compounds that feature at least four guanidino groups (GFA = guanidino-functionalized aromatic compounds) as a new class of strong organic electron donors and redox-active complex ligands.[17,18] Two representatives are ttmgb [1,2,4,5-tetrakis(tetramethylguanidino)benzene] and ttmgn [1,4,5,8-tetrakis(tetramethylguanidino)naphthalene] (see Scheme 2). The ligand ttmgb was shown to form stable complexes not only in its neutral form, but also upon one-electron oxidation to the radical cation[19] or two-electron oxidation to the dication.[20] Herein we use the ttmgb ligand for the syntheses of dinuclear Co^{II} and Ni^{II} complexes.

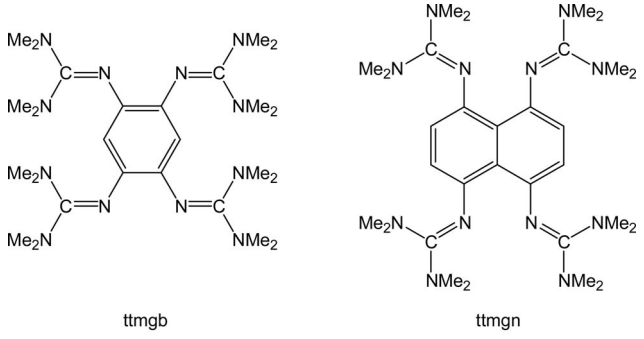

[(ttmgb){$CoCl_2$}$_2$], **6**
[(ttmgb){$Co(OAc)_2$}$_2$], **7**
[(ttmgb){$NiCl_2$}$_2$], **8a**
[(ttmgb){$NiBr_2$}$_2$], **8b**
[(ttmgb){Ni(acac)$_2$}$_2$], **9**

Scheme 2.

Results and Discussion

In the following the syntheses, structural characterization, analysis by quantum chemical calculations, magnetism, and paramagnetic NMR spectra of mononuclear as well as dinuclear Ni and Co complexes of the ligands btmgb, bdmegb, btmgmpy, and ttmgb will be described.

Syntheses and Structural Characterization

btmgmpy

Starting from 2,6-bis(hydroxymethyl)pyridine, one obtains 2,6-bis(bromomethyl)pyridine by bromination with PBr_3 (Scheme 3).[21] A subsequent Gabriel reaction provides the diamine as a white solid.[22] In analogy to the syntheses of other guanidine systems, this diamine can be treated with activated tetramethylurea (TMU) to obtain the desired ligand.[16]

Up to now, the molecular structure of the ligand has not been reported and is therefore included in this work. A visualization can be found in the Supporting Information. The bond lengths in the aromatic system are in good agreement with other 2,6-substituted pyridines, namely, 134.4 (N1–C1), 137.9 (C1–C2), and 138.2 pm (C2–C3). The guanidino units exhibit bond lengths of 128.4 pm for the C–N imine bond (C7–N2) as well as 139.0 (C7–N3) and 138.4 pm (C7–N4) for the amine bonds. These bond lengths are in a typical range for guanidines. Furthermore, the guanidino units are oriented in opposite directions with respect to the pyridine plane. In the crystal, the ligand adopts a full-*trans* geometry, which means that all bonds between both guanidino units exhibit *trans* conformation. Thus the two imino nitrogen donor atoms of the guanidino groups are pointing away from the desired κ^3-coordination sphere. As a consequence, the system needs to rearrange prior to establishing κ^3 coordination with a metal center.

Mononuclear Co Complexes

The two mononuclear complexes [(btmgb)$CoCl_2$] (**1**) and [(btmgb)$Co(OAc)_2$] (**2**) were synthesized by reaction between btmgb and $CoCl_2$ in acetonitrile at 70 °C (in the case of **1**) or $Co(OAc)_2$ in ethanol at room temp. (in the case of **2**). The two complexes were crystallized from solutions in thf. The molecular structures as derived from XRD analysis are depicted in Figure 1. The Co^{II} ions are fourfold coordinated in halide complex **1**. With 113.1°, the Cl–Co–Cl angle in **1** is close to the ideal tetrahedral angle. Complex **2** prefers a distorted trigonal-bipyramidal coordination in which one of the OAc ligands is bound by two and the other only by one of the O atoms. The Co–N1/Co–N2 distances measure 202.8/200.5 pm for **1** and 201.6/205.4 pm for **2**. The N1–Co–N2 bite angles are almost identical in both compounds (83.30° in **1** and 82.13° in **2**). On the other hand,

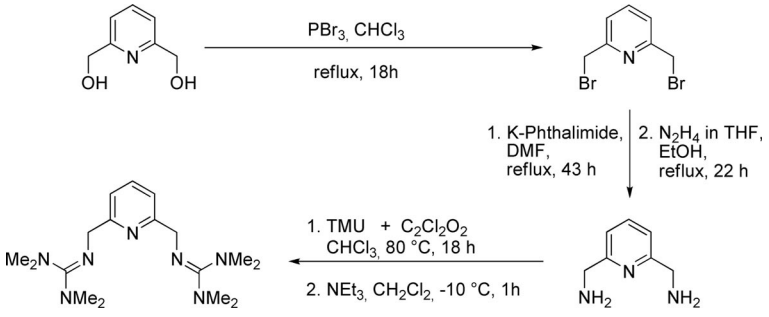

Scheme 3.

the configuration of the tetramethylguanidino groups is different in **1** and **2**. Hence, the two guanidino groups adopt a *cis*-type conformation in crystals of complex **1** (see Figure 1). A similar conformation was also previously observed in the mononuclear Ni complexes [(btmgb)NiX_2] and [(btmgn)NiX_2] (X = Cl and Br).[7] On the other hand, a *trans*-type conformation is adopted in **2**. Quantum chemical calculations were carried out to obtain information about the energy difference between the two possible conformations (*cis* or *trans*) of the two guanidino groups in complex **1**. By using the BP86 functional in combination with the SV(P) basis set, an energy difference of 16.9 kJ mol^{-1} in favor of the *trans* configuration is predicted, whereas the B3LYP functional yields 11 kJ mol^{-1}. This indicates the presence of an equilibrium between both conformers in solution.

Finally, we synthesized the complex [(bdmegb)$CoCl_2$] (**3**) by reaction of $CoCl_2$ with bdmegb in acetonitrile at room temp. Blue crystals could thus be obtained after workup from a solution in thf (Figure 2). This system displays some structural similarities to **1**. The bridging ethylene subunits of each guanidino group force the formed heterocycle into an envelope form. The Co–N1/Co–N4 distances measure 202.6 and 201.2 pm, respectively. Furthermore, with 82.9°, the N4–Co–N1 bite angle is close to that in **1**. Complex **3** exhibits, like **1**, a *cis*-type conformation of the guanidino units in the crystalline phase.

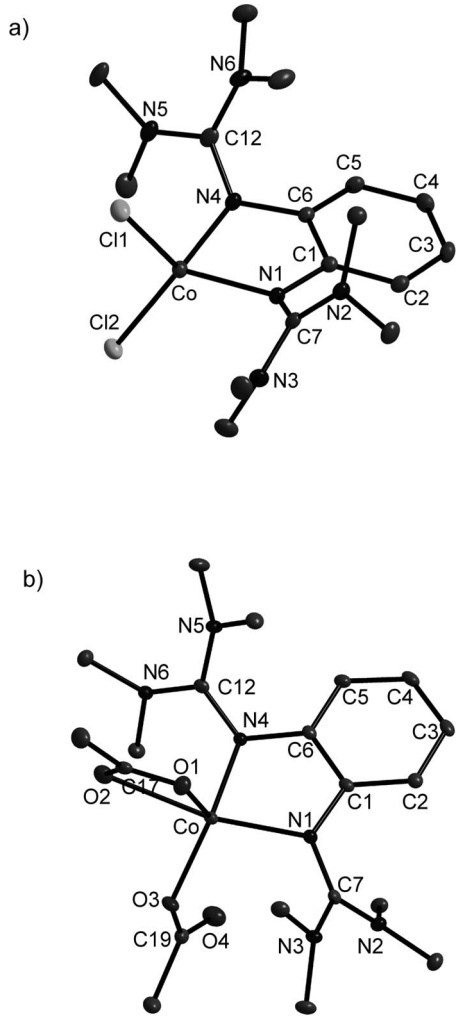

Figure 1. Molecular structures of complexes **1** (a) and **2** (b). Thermal ellipsoids are drawn at the 50% probability level. Selected structural parameters (bond lengths in pm, bond angles in °) for **1**: Co–N1 2.0275(15), Co–N4 2.0046(15), Co–Cl1 2.2539(6), Co–Cl2 2.2514(6), N1–C1 1.415(2), N1–C7 1.334(2), N2–C7 1.359(2), N3–C7 1.350(2), N4–C6 1.414(2), N4–Cl2 1.337(2), N5–Cl2 1.345(2), N6–Cl2 1.350(2); N1–Co–N4 83.30(6), Cl1–Co–Cl2 113.14(2), C1–N1–C7 120.38(15), C6–N4–Cl2 120.39(15). Selected structural parameters (bond lengths in pm, bond angles in °) for **2**: Co–N1 2.0541(16), Co–N4 2.0155(15), Co–O1 2.0457(14), Co–O2 2.3812(15), Co–O3 1.9612(14), Co···O4 310.0(3), N1–C1 1.414(2), N1–C7 1.323(2), N2–C7 1.368(2), N3–C7 1.352(2), N4–C6 1.410(2), N4–C12 1.343(2), N5–C12 1.356(2), N6–C12 1.346(2); N1–Co–N4 82.13(6), C1–N1–C7 121.28(15), C6–N4–C12 120.37(15).

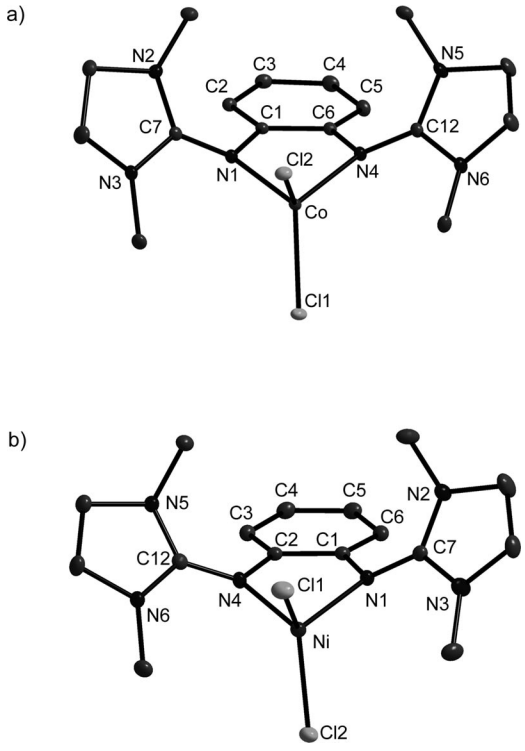

Figure 2. Molecular structures of complexes **3** and **4a**. Ellipsoids are drawn at the 50% probability level. Selected structural parameters (bond lengths in pm, bond angles in °) for **3**: Co–N1 2.0125(10), Co–N4 2.0255(10), Co–Cl1 2.2654(5), Co–Cl2 2.2608(6), N1–C1 1.4102(14), N1–C7 1.3335(14), N2–C7 1.3461(14), N3–C7 1.3484(14), N4–C6 1.4214(14), N4–C12 1.3252(14), N5–C12 1.3520(15), N6–C12 1.3602(14); Cl1–Co–Cl2 109.485(17), N1–Co–N4 82.95(4). Selected structural parameters (bond lengths in pm, bond angles in °) for **4a**: Ni–N1 1.9996(18), Ni–N4 1.9925(17), Ni–Cl1 2.2537(8), Ni–Cl2 2.2513(7), N1–C1 1.421(3), N1–C7 1.320(2), N2–C7 1.353(3), N3–C7 1.349(3), N4–C2 1.415(3), N4–C12 1.322(3), N5–C12 1.357(3), N6–C12 1.352(3); Cl1–Ni–Cl2 126.16(3), N1–Ni–N4 83.56(7).

Mononuclear Ni Complexes

Complexes [(bdmegb)NiX_2] [X = Cl (**4a**), X = Br (**4b**)] can be synthesized by treatment of bdmegb with the corresponding NiX_2–1,2-dimethoxyethane (dme) adduct in

dichloromethane at –80 °C. Crystals of **4a** and **4b** suitable for X-ray determination were grown from a dichloromethane solution overlaid with *n*-hexane (see Figure 2 for **4a** and the Supporting Information for **4b**). Like in Co complex **3**, in **4a** the metal center is displaced from the phenylene plane (by 24.2°). Both guanidino groups adopt a *cis*-type conformation, and again the heterocycle is forced into an envelope form. The N1–Ni–N4 bite angle is found to be 83.6°, which is of the same order as that for the [(btmgb)$NiCl_2$] complex. With 126.2°, the Cl–Ni–Cl angle is significantly larger than the Cl–Co–Cl angle in the corresponding Co complex. As shown in a previous work,[7] complexes [(btmgb)NiX_2] and [(btmgn)NiX_2] (X = Cl or Br) also feature X–Ni–X angles that are significantly larger than the ideal tetrahedral angle; all adopt values close to 130°.[7] Such large Cl–Ni–Cl angles are found not only in the case of aromatic bis(guanidine) ligands, but also for other strong donor ligands. To obtain more information about the Cl–Ni–Cl bond angle in compounds of the general formula [L_2NiCl_2] (L being a nitrogen donor), we carried out a statistic search of the Cambridge Structural Database (CSD).[23] Only structures with four-coordinate Ni (featuring two Ni–N and two Ni–Cl bonds) were considered, narrowing down the number of hits to 42 (including the structures presented herein). The results (see Supporting Information for a graphical presentation) show that the majority of the complexes prefer angles between 125 and 135° in the crystalline phase. Quantum chemical density functional theory (DFT) calculations for the molecules in the gas phase predict a much smaller angle (close to 110°), but also point to a soft Cl–Ni–Cl bending potential.[7] For comparison, the Cl–Co–Cl angles in the corresponding Co complexes are all significantly smaller. Therefore, the large bond-angle value is unlikely to result from electrostatic repulsion between the chlorido ligands. Moreover, the statistics seem to argue against crystal-packing effects. One possible approach is the mixing of electronically excited states into the ground state. The presence of considerable zero-field splitting (see the analysis of the molecular magnetism below) in these $S = 1$ systems is of interest in this context. Moreover, the dinuclear complex [(ttmgb)($NiCl_2$)$_2$] ($S = 0$ ground state due to antiferromagnetic exchange) displays a significantly smaller Cl–Ni–Cl bond angle (107.0°; see below). More theoretical work is necessary to shed light on this particular point.

Further examples of mononuclear Ni complexes are the compounds [(btmgmpy)NiX_2] [X = Cl (**5a**), X = Br (**5b**)]. They can be synthesized by reaction of the btmgmpy ligand with the corresponding NiX_2–dme adduct in dichloromethane at –80 °C. In analogy to **4**, crystals were grown from a dichloromethane solution overlaid with *n*-hexane. The molecular structure of **5a** is illustrated in Figure 3. As discussed above, to act as tridentate N-ligand, the btmgmpy molecule has to rearrange from its full-*trans* to an s-*cis* isomeric form with regards to the C1–C6/C5–C12 bond. As a consequence, two enantiomeric forms exist in the crystal. The most remarkable difference between this complex and the other mononuclear Ni complexes certainly is the coordination mode. Hence, the Ni center in **5a** is fivefold coordinated in a trigonal-bipyramidal fashion. However, the Cl–Ni–Cl angle measures only 152.6°. In comparing the Ni–N bond lengths, one observes that the pyridine nitrogen atom is coordinated at a distance of 196.3 pm (Ni–N1), whereas both guanidino nitrogen atoms display a bond length of 210.5 pm. Like in **2**, the guanidino units adopt a *trans* conformation in the crystalline phase, which until now has not been observed in any of the other bis(guanidine)nickel complexes. As a consequence of the bite angle and the flexibility in the backbone, the pyridine plane is distorted by 14.7° with respect to the N5–Ni–N2 plane.

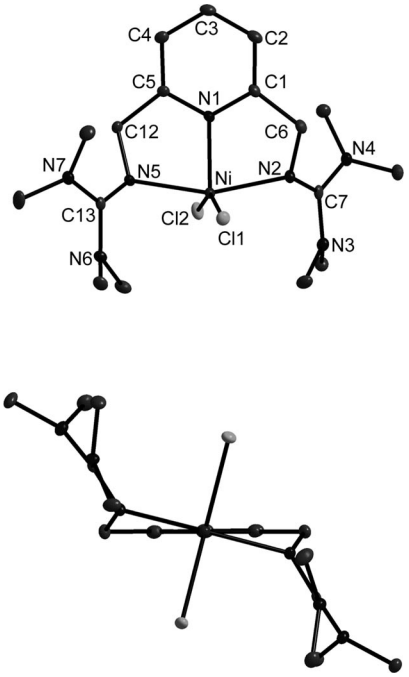

Figure 3. Molecular structure of the complex **5a**. Ellipsoids are drawn at the 50% probability level. Selected structural parameters (bond lengths in pm, bond angles in °) for **5a**: Ni–N1 1.9635(18), Ni–N2 2.1063(17), Ni–N5 2.1050(18), Ni–Cl1 2.3280(8), Ni–Cl2 2.3197(7), N2–C7 1.308(3), N3–C7 1.365(3), N4–C7 1.371(3), N5–C12 1.466(3), N5–C13 1.307(3), N6–C13 1.358(3), N7–C13 1.370(3); Cl1–Ni–Cl2 152.62(3), N2–Ni–N5 159.52(7), N1–Ni–N2 79.65(7), N1–Ni–N5 79.87(7).

The ability of the btmgmpy ligand to coordinate either in a κ^3 or κ^2 mode was further analyzed by quantum-chemical calculations. These calculations found minima for κ^3 coordination with a *cis*- as well as a *trans*-type arrangement of the guanidino groups. They also provided a minimum structure for κ^2 coordination, in which one guanidino arm is turned away from the coordination sphere. Figure 4 displays the three minimum coordination geometries in both singlet and triplet electronic states. In all cases, the triplet states were favored over the singlet states. In the case of κ^3 coordination, the *cis*-type arrangement of the guanidino groups, as observed in other Ni^{II}–bis(guanidine) complexes, is disfavored by not more than 8 kJ mol^{-1} over the *trans*-type arrangement (which is also observed in this case) according to our calculations. The calculations indicate that κ^2 coordination is indeed disfavored energetically by 32.5 kJ mol^{-1}.

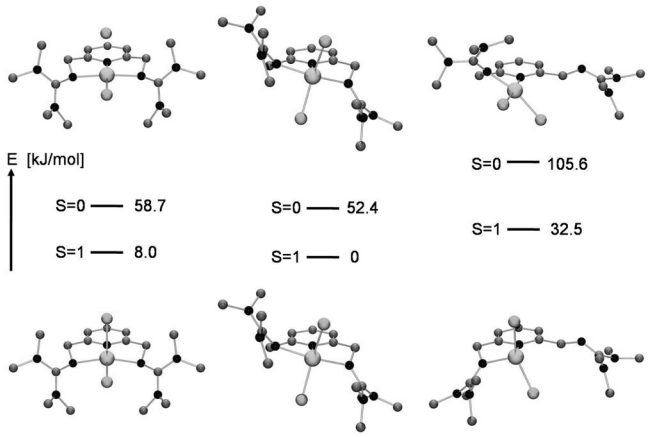

Figure 4. DFT-optimized structures of the possible coordination geometries of **5a** with spin multiplicities of $S = 1$ and $S = 0$ [B3LYP/def2-SV(P)].

Dinuclear Co and Ni Complexes

Dinuclear Co complexes were synthesized by treating the GFA ligand ttmgb with CoX_2 (X = Cl or OAc). The complex $[(ttmgb)\{CoCl_2\}_2]$ (**6**) has already been reported by us in an earlier publication.[18] The dinuclear Co complex $[(ttmgb)\{Co(OAc)_2\}_2]$ (**7**) was crystallized from a solution in thf. The molecular structure is visualized in Figure 5a. Two independent molecules are found within the unit cell with different acetato ligand bonding modes. Both molecules are presented in Figure 5b. In one of these, three of the OAc ligands are only κ^1-bonded through one O atom to the Co center, thereby leading to one tetra- and one pentacoordinate Co^{II} ion. In the second molecule, one Co^{II} atom is hexa- and the other tetracoordinated.

In addition, we synthesized the three dinuclear Ni complexes $[(ttmgb)\{NiCl_2\}_2]$ (**8a**) $[(ttmgb)\{NiBr_2\}_2]$ (**8b**) and $[(ttmgb)\{Ni(acac)_2\}_2]$ (acac = acetylacetonato) (**9**). Of these, **8a** and **8b** feature fourfold-coordinated, and complex **9** sixfold-coordinated Ni^{II} centers. Crystals suitable for an XRD analysis were obtained for complexes **8a** and **9** (see Figures 6 and 7). The structure of **8a** is similar to that of the Co^{II} complex **6**. Around each Ni^{II} center, the guanidino groups are arranged in a *cis*-type conformation, whereas the metal atoms are located at opposite sides of the aromatic plane. In comparison to **6**, the tetrahedral coordination sphere in **8a** is distorted by an angle of 84.0°. Interestingly, the Cl–Ni–Cl angles (107.0°) are much smaller than in the mononuclear complex $[(btmgb)NiCl_2]$.[7]

Figure 6 also includes a Vis/NIR spectrum for **8a**. At least four absorptions are visible in the spectral range 450–1500 nm, with maxima of absorptions around 480, 575, 685, and 1025 nm. To analyze the excitation spectrum of **8a**, some density functional calculations were performed. Two states, the high-spin ^5A state with the parallel orientation of the local spins of the two Ni^{II} atoms and the broken symmetry state, were investigated. The structures were optimized with the BP86 functional and the def2-SV(P) basis set by using the approximate resolution of the identity (RI). Both states have similar energies (the high-spin ^5A state be-

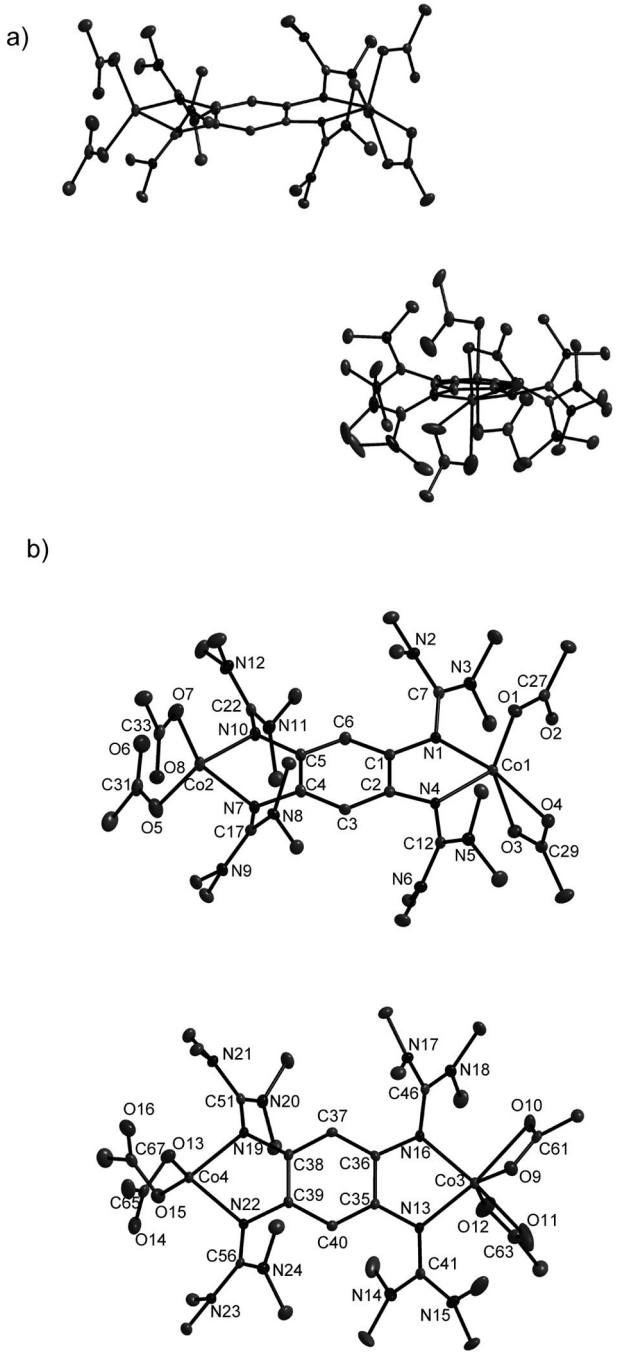

Figure 5. Molecular structure of complex **7**. (a) Relative orientation of the two molecules in the crystal. (b) Illustration of the two slightly different molecules with atom numbering. Thermal ellipsoids are drawn at the 50% probability level. Selected structural parameters (bond lengths in pm, bond angles in °) for **7**: Co1–N1 2.069(2), Co1–N4 2.082(2), Co1–O1 2.0722(19), Co1···O2 2.287(2), Co1–O3 2.1002(18), Co1–O4 2.240(2), Co2–N7 2.037(2), Co2–N10 2.041(2), Co2–O7 1.988(2), Co2···O8 273.1(3), Co2–O5 1.965(2), Co2···O6 280.9(3), Co3–N13 2.070(2), Co3–N16 2.049(2), Co3–O9 2.0801(18), Co3–O10 2.290(2), Co3–O11 2.186(3), Co3–O12 2.276(3), Co4–N19 2.055(2), Co4–N22 2.052(2), Co4–O13 2.007(2), Co4···O14 255.4(3), Co4–O15 2.032(2), Co4···O16 249.6(2), N1–C1 1.423(3), N1–C7 1.337(3), N4–C2 1.414(3), N4–C12 1.330(3), N7–C4 1.417(3), N7–C17 1.337(3), N10–C5 1.419(3), N10–C22 1.328(3), N13–C35 1.419(3), N13–C41 1.325(4), N16–C36 1.421(3), N16–C46 1.331(3), N19–C38 1.419(3), N19–C51 1.328(3), N22–C39 1.415(3), N22–C56 1.341(3); N1–Co1–N4 81.30(8), N7–Co2–N10 82.42(9), N13–Co3–N16 81.74(9), N19–Co4–N22 82.33(9).

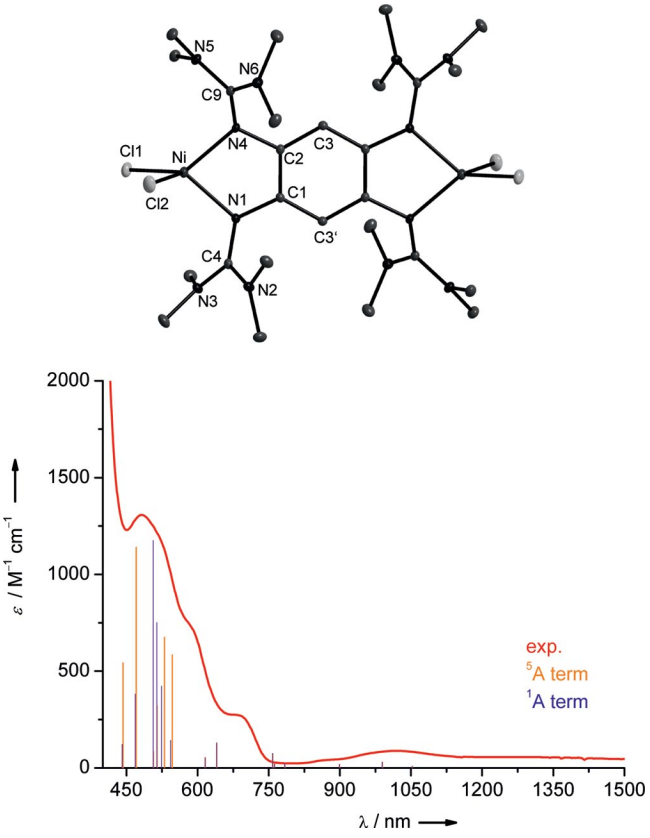

Figure 6. Molecular structure of complex **8a**. Thermal ellipsoids are drawn at the 50% probability level. Selected structural parameters (bond lengths in pm, angles in °): Ni–Cl1 2.2374(8), Ni–Cl2 2.2542(7), Ni–N1 1.9867(15), Ni–N4 2.0040(14), N1–C4 1.338(2), N4–C9 1.326(2), N1–C1 1.411(2), N4–C2 1.417(2), C1–C2 1.403(2), C1–C3′ 1.394(2), C2–C3 1.395(2); Cl1–Ni–Cl2 106.97(2), N1–Ni–N4 83.22(6). In addition, the figure shows the Vis/NIR spectrum of this compound, together with a simulation on the basis of quantum chemical calculations (see text).

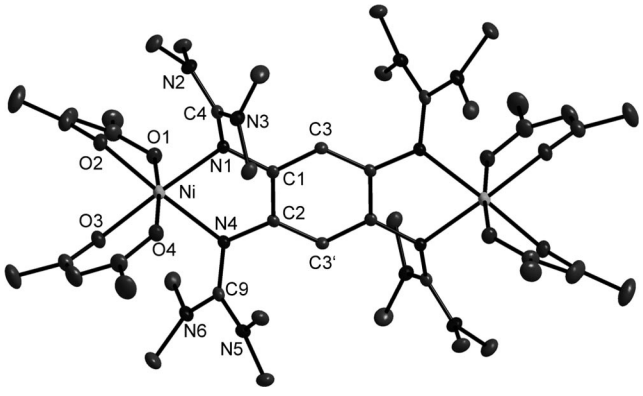

Figure 7. Molecular structure of complex **9**. Thermal ellipsoids are drawn at the 50% probability level. Selected structural parameters (bond lengths in pm, angles in °): Ni–O1 2.027(2), Ni–O2 2.057(2), Ni–O3 2.043(2), Ni–O4 2.058(2), Ni–N1 2.104(2), Ni–N4 2.129(2), N1–C1 1.410(3), N1–C4 1.327(3), N2–C4 1.358(3), N3–C4 1.360(4), N4–C2 1.413(3), N4–C9 1.319(3), N5–C9 1.373(4), N6–C9 1.360(3), C1–C2 1.409(3), C1–C3 1.400(3), C2–C3′ 1.394(3); N1–Ni–N4 79.61(8), O1–Ni–O2 88.69(9), O3–Ni–O4 87.68(9), O1–Ni–O4 173.61(8), C1–N1–Ni 113.08(16), C1–N1–C4 119.4(2), C2–N4–Ni 112.40(16), C2–N4–C9 119.2(2).

ing energetically higher by 0.0096 kJ mol^{-1}), thus indicating very small magnetic coupling between the two Ni^{II} atoms. For the optimized structures, the energies and transition moments of the excited states were obtained by subsequent calculations with the B3LYP functional and the same basis set in the framework of time-dependent density functional theory.[24] The most likely candidate for a d–d transition is the broad and relatively weak absorption around 1025 nm. The calculations predicted an electronic transition at around 1000 nm (for both states). The inspection of the orbital contributions confirms the dominant involvement of metal d-orbitals. In the Supporting Information, the isodensity surfaces for some of the involved spin orbitals are visualized.

For complex **9**, the Ni^{II} ions are surrounded by the ligands in a distorted octahedral geometry. Both oxygen atoms from each acac ligand are coordinated to the Ni^{II} centers, thereby resulting in two chiral centers. Whereas the Λ-isomer is realized at Ni1, at Ni2 the Δ-isomer is found. The metal centers in **9** are positioned within the aromatic plane.

Magnetic Measurements

To obtain insight into the magnetism of the presented mono- and dinuclear Co and Ni complexes, we performed superconducting quantum interference device (SQUID) measurements in the solid state within a temperature range from 2 to 300 K. Furthermore, we studied the magnetism of the complexes **8a**, **8b**, and **9** in solution at room temperature with the help of the Evans method.[25] Examination by means of electron paramagnetic resonance (EPR) at the X-band frequency could not be accomplished because of the strong zero-field splitting (ZFS), which is inherent to all complexes.

By applying the Evans method, the molar magnetic susceptibility (χ_M^p) was obtained by Equation (1).

$$\chi_M^p = \frac{3 \cdot \Delta f \cdot M^p}{4\pi \cdot f_0 \cdot c^p} - \chi_M^{dia} \quad (1)$$

Herein, ($^3/_4\pi$) is a geometric prefactor that is valid for magnets with vertical magnetic-field axis, f_0 is the operating frequency of the spectrometer [Hz], Δf the solvent shift relative to the shift of the pure solvent [Hz], c^p the concentration of the solute [g cm^{-3}], and M^p the molecular mass of the dissolved paramagnetic compound [g mol^{-1}]. The molar diamagnetic contribution (χ_M^{dia}) of the compound [cm^3 mol^{-1}] was estimated on the basis of the diamagnetic susceptibilities and constitutive Pascal corrections and subtracted. Thereby, we obtained values of 3.36, 3.55, and 3.33 μ_B for the magnetic moment μ_{eff} of the complexes **8a**, **8b**, and **9**, respectively (CD_2Cl_2, 303 K).

The temperature-dependent magnetic direct-current (dc) susceptibilities of the eleven complexes **1**, **2**, **4a**, **4b**, **5a**, **5b**, **6**, **7**, **8a**, **8b**, and **9** in the solid state were derived from a series of SQUID measurements. We obtained the axial ZFS parameter D for the mononuclear complexes and the iso-

tropic coupling parameter J for the dinuclear complexes by curve fitting. For the fit functions of the mononuclear systems, the Hamiltonian according to Equation (2) was used to describe the spin–spin interaction along the axial direction.

$$\hat{H}_{ZFS} = D(\hat{S}_z^2 - \frac{1}{3}\hat{S}^2) \quad (2)$$

By determination of the van Vleck coefficients, the molar magnetic susceptibility can be calculated from the van Vleck equation. For the mononuclear Ni^{II} complexes (S = 1), it results in Equation (3).[26]

$$\chi_M = \frac{2N_A\mu_B^2}{3k_B(T-\Theta_{CW})} g^2 \frac{e^{-D/k_BT} + 2\frac{k_BT}{D}\left(1-e^{-D/k_BT}\right)}{1+2e^{-D/k_BT}} + TIP \quad (3)$$

For the mononuclear Co^{II} complexes (S = 3/2), one obtains Equation (4).

$$\chi_M = \frac{N_A\mu_B^2}{12k_B(T-\Theta_{CW})} g^2 \left(\frac{1+9e^{-2D/k_BT}}{1+e^{-2D/k_BT}} + 8\cdot\frac{1+\frac{3k_BT}{4D}\left(1-e^{-2D/k_BT}\right)}{1+e^{-2D/k_BT}} \right) + TIP \quad (4)$$

Herein N_A is the Avogadro constant, μ_B is the Bohr magneton, g is the isotropic Landé factor, D is the axial zero-field splitting parameter, k_B is the Boltzmann constant, and TIP the temperature-independent paramagnetism. By employing a Curie–Weiss temperature (Θ_{CW}), possible intermolecular interactions were also taken into account. Fitting the experimentally obtained data results in the values listed in Table 1.

Table 1. Fitting parameters obtained by applying Equations (3) and (4) for the mononuclear complexes.

	1	**4a**	**4b**	**5a**	**5b**
g	2.10	2.12	2.29	2.06	2.10
D [cm^{-1}]	15.3	40.2	32.0	2.5	2.9
Θ_{CW} [K]	0.15	0.67	0.44	–2.54	–2.28
TIP [10^{-3} cm^3 mol^{-1}]	2.0	2.63	0.54	0.00	0.07

In the case of the dinuclear complexes, magnetization data were collected at an applied field of 0.5, 1, 2, 3, 4, and 5 T and corrected for the underlying diamagnetism. The program julX was then used for the simulation and analysis of the magnetic susceptibility data,[27] based on the spin-Hamiltonian operator according to Equation (5).

$$\hat{H} = g\beta\hat{\vec{S}}\cdot\vec{B} + D\left(\hat{S}_z^2 - \frac{1}{3}S(S+1) + E/D(\hat{S}_x^2 - \hat{S}_y^2)\right) \quad (5)$$

Figure 8 shows as an example the χT versus T curve derived for the mononuclear Co complex **1**, and Figure 9 shows the curves for the dinuclear Ni complexes **8a** and **9**. The values of the fit parameters for all magnetic curves (except for **2** and **7**; see discussion below) are included in Table 2. The coupling constants of all dinuclear complexes are very small. As a consequence of the different coordination geometries, the D parameter is much smaller for **9** (octahedral coordination) than for **8a** or **8b** (tetrahedral coordination).

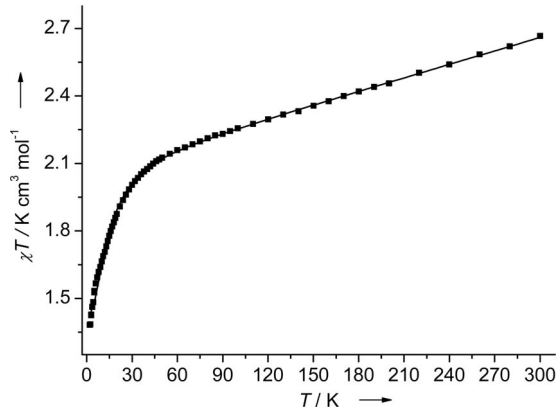

Figure 8. Dependence of χT on the temperature as derived from SQUID magnetic measurements for complex **1**, together with a fit according to Equation (4) (solid line).

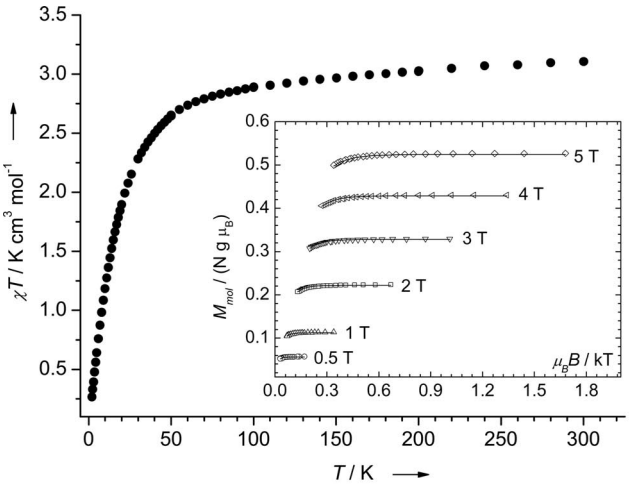

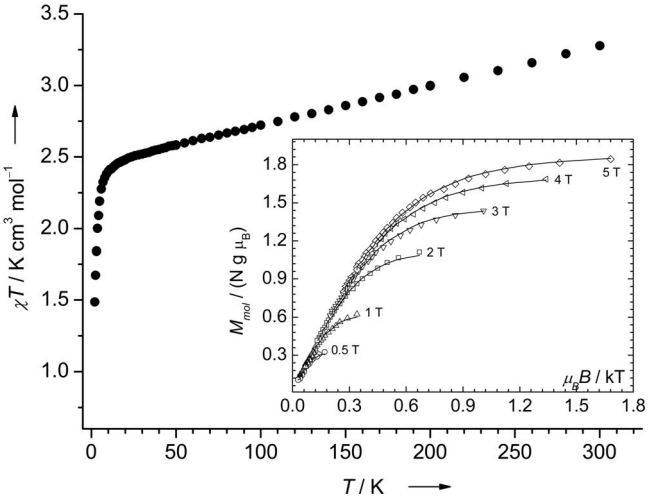

Figure 9. χT versus T plots for complexes **8a** and **9** as derived from SQUID magnetic measurements and temperature dependence of the molar magnetization at B = 0.5, 1, 2, 3, 4, and 5 T sampled on a $1/T$ inverse-temperature scale (inset). The solid lines are the result of a global spin-Hamiltonian simulation (see text).

Table 2. Fitting parameters obtained for the dinuclear complexes.

	6	8a	8b	9
$g_1 = g_2$	2.12	2.09	2.09	2.20
J [cm^{-1}]	2.73	0.68	0.48	–0.043
$D_1 = D_2$ [cm^{-1}]	16.0	30.3	33.1	4.4
$E/D_1 = E/D_2$ [cm^{-1}]	0.09	0.33	0.50	0.00
Θ_{CW} [K]	–1.558	0.014	0.09	0.093
TIP [10^{-6} cm^3 mol^{-1}]	0.5	0.1	30.3	1.2

In the case of the two Co–acetato complexes **2** and **7**, the magnetic curve can be fitted by the Curie–Weiss law for temperatures above approximately 50 K. The Curie constant and Weiss temperature are 2.40 mol cm^{-3} and –10.3 K for **2** and 6.99 mol cm^{-3} and –12.2 K for **7**, respectively. We observed a significant influence of the applied magnetic field strength on the χT value for temperatures below approximately 15 K (see Figure 10). For complex **2**, the χT values as measured at 500 G first decrease and reach a minimum of 1.89 K cm^3 mol^{-1} at 20 K. This decrease can be explained by the onset of antiferromagnetic exchange between the molecules. At lower temperatures, the χT value jumps up and reaches a value of 2.24 K cm^3 mol^{-1} at 9 K before it rapidly decreases. For complex **7** we measured χT versus T curves for nine different magnetic fields in the range 50–1000 G. Until around 7 K all curves are similar, with the χT value slowly decreasing to around 3.4 K cm^3 mol^{-1}. At lower temperatures, the χT value for measurement at 50 G jumps up to 12 K cm^3 mol^{-1} at 4.5 K before it sharply decreases. With increasing field the temperature of the maximum shifts to lower values, and the χT value at the maximum decreases significantly. Hence at 1000 G the maximum occurs at 3.8 K, with χT being 4.7 K cm^3 mol^{-1} at this maximum.

The magnetic curves were reproduced several times with different samples (see also the plots for the magnetization as a function of the applied field in the Supporting Information) to prove that they indeed describe the magnetism of compounds **2** and **7**. Impurities can be excluded as being responsible for this effect. The magnetic properties at low temperatures point to intermolecular magnetic interactions.

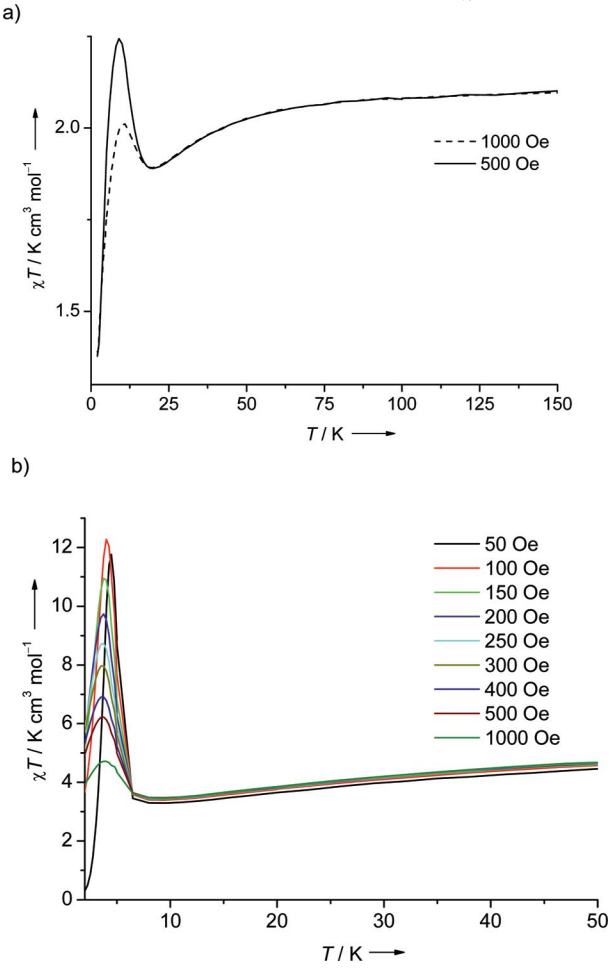

Figure 10. χT versus T plots for complexes **2** and **7** as derived from SQUID magnetic measurements.

Quantum Chemical Calculations on the Co Complexes

Quantum chemical calculations were carried out for Co complexes **1**, **2**, **6**, and **7**. The structures of the mononuclear complexes (**1** and **2**) were optimized by using the B3LYP and BP86 functional. As anticipated, for complex **1** both functionals predict a quartet state to be of lowest energy. The sextet state is predicted at much higher energy. Values of 222 and 263 kJ mol^{-1} above the quartet state are obtained by using the BP86 and the B3LYP functional, respectively. The energy separation between the quartet state and a state with M_S = 1, amounts to 64 (BP86) or 96 kJ mol^{-1} (B3LYP). In fact, the latter state is not a doublet state; the values for $<S^2>$ are 1.41 (BP86) and 1.74 (B3LYP). For complex **2**, the calculations yield a similar energetic order. However, the separation between the M_S = 1 and the quartet term is significantly smaller: 28 (BP86) and 65 kJ mol^{-1} (B3LYP), whereas the sextet term lies 215 (BP86) or 251 kJ mol^{-1} (B3LYP) above the quartet term.

In the case of the dinuclear clusters (**6** and **7**), septet terms with a parallel coupling of the spins of the two quartet Co^{II} centers and broken-symmetry states with an antiparallel alignment were considered in the calculations with the B3LYP functional. For complex **6**, these calculations predict the broken-symmetry state and the septet term to exhibit virtually the same energy: the broken-symmetry term is higher than the septet term by (an insignificant) 0.004 kJ mol^{-1}, which transforms into a value for J of 0.068 cm^{-1} ($\mathbf{H} = -J\mathbf{S}_1\mathbf{S}_2$) that indicates an extremely weak J coupling between the two Co centers. The value is close to the estimate of –0.61 cm^{-1} from fitting the magnetic curve for complex **6**. Similarly for complex **7**, the energy of the broken-symmetry state and the septet term are virtually identical. (The energy of the broken-symmetry term is higher by 0.39 kJ mol^{-1}.)

In the case of chlorido complexes **1** and **6**, the calculated structures are in excellent agreement with those determined by X-ray diffraction. For acetato complex **2**, somewhat larger differences are observed. The crystal structure shows

values for the Co–O distances of 196.1, 204.6, 238.1, and 310.0 pm. In contrast, the B3LYP calculations yield two shorter and two longer values of 212 and 227 pm. Hence, within the crystal structure one acetato ligand is κ^2-coordinated, the other is κ^1-coordinated, but in the lowest-energy B3LYP structure both acetato ligands show κ^2-coordination. Nevertheless, also by B3LYP, a structure is found that has one acetato ligand in κ^1-coordination, which corresponds to the crystal structure. It has an energy higher by 8 kJ mol^{-1} than the κ^2-isomer. Most likely, packing effects are responsible for the difference between the calculated gas phase and the crystal structure. In the case of dinuclear complex **7**, the calculations predict for each of the Co ions two short Co–O bond lengths of 212 pm and two longer ones of 227 pm. Thus, in this case again the calculations argue for κ^2-coordination of the acetato ligands and sixfold coordination of the metal ions. This is in agreement with the coordination on one of the Co sites of each dinuclear complex in the crystal structure. However, the variations in the Co–O distances are larger for the crystal structure: 207.2, 210.0, 224.0, 228.7, and 208.0, 218.6, 227.6, 229.0 pm. For the other Co site of each of the two complexes in the crystal structure, the difference between the shorter and the longer Co–O distance is more pronounced: 200.7 and 203.2 versus 249.6 and 255.4 pm, or even 198.8 and 196.5 versus 273.1 and 280.9 pm. The simultaneous presence of these different metal–ligand distances in the crystal structure points to only small energetic differences between the different coordination modes. Hence, again crystal-packing effects are likely to play the dominating role.

Paramagnetic NMR Spectroscopic Studies

Here we discuss NMR spectroscopic data for one of the complexes, namely, **3**, which gave good-quality spectra. Recently, we reported on the detailed analysis of the paramagnetic variable-temperature (VT) NMR spectra of a series of mononuclear Ni^{II} complexes with chelating guanidine ligands.[28] Figure 11 displays a $^1J_{C,H}$ correlation plot of **3** measured with a 600 MHz machine. This spectrum will be discussed from low- to highfield $\delta(^{13}C)$ values. Two resonances are strongly lowfield-shifted at δ = 439.6 and 407.6 ppm. The first one splits into a doublet, interacts with the signal at δ = 22.15 ppm in the ^{1}H NMR spectrum, and thus can be assigned to one of the aromatic carbon atoms. The second one (singlet) does not interact with any other nucleus and can be allocated to one of the quaternary carbon atoms. A similar pattern can be observed for the two resonances at δ = 239.9 and 219.5 ppm: the former one is a singlet, whereas the latter splits into a doublet. In analogy to the argumentation above, these signals can be assigned to one of the quaternary carbon atoms and to one of the aromatic carbon atoms, respectively. In agreement with such an assignment, a cross-peak with the resonance at δ = 18.82 ppm in the ^{1}H NMR spectrum is clearly visible for the doublet, whereas a correlation is absent in the case of the quaternary carbon atom. In the region between δ = 20 and –10 ppm, one observes a triplet at δ = 21.8 ppm, which interacts with two resonances of the ^{1}H NMR spectrum, located at δ = 27.70 and 25.61 ppm. These signals were assigned to the ethylene bridge of the guanidino groups. Thus, only with the aid of this ^{1}H–^{13}C correlation was it possible to assign the signals unambiguously. In principle, this pattern can be explained by a symmetry plane that intersects the ethylene C–C bond. However, in full agreement with the corresponding Ni^{II} complexes, a better explanation is the fluxional behavior by fast movement of the metal center from one side of the plane defined by the phenyl ring to the other side. This movement was confirmed in the case of cationic complexes of $AlMe_2$,[6] for which splitting of the methyl group signals can be observed. Finally, the signal at δ = 18.1 ppm splits into a broad quartet, which corresponds to the ^{1}H resonance at δ = 0.65 ppm, and consequently belongs to the NMe groups. A definite assignment of the aromatic and quaternary carbon atoms was possible with the aid of DFT calculations (B3LYP/def2-TZVP), especially with the knowledge of the spin density at certain nuclei. Therefore, we used the same theoretical background as described for the Ni^{II} complexes.[28,29] By subtracting the diamagnetic chemical shift from the observed chemical shift of **3**, one obtains the paramagnetic term ($\delta^{exptl.}_{HF,T}$), which can directly be compared with the calculated term of the Fermi contact ($\delta^{calcd.}_{con}$) (see Table 3). For this purpose, we used the analogous Zn complex [(bdmegb)$ZnCl_2$] as diamagnetic reference. For the aromatic carbon atoms, this method matches quite well and the computed values correlate with the experimentally obtained ones. For the quaternary carbon atoms, this method fails to give a quantitative prediction, because it is based on the assumption that other ef-

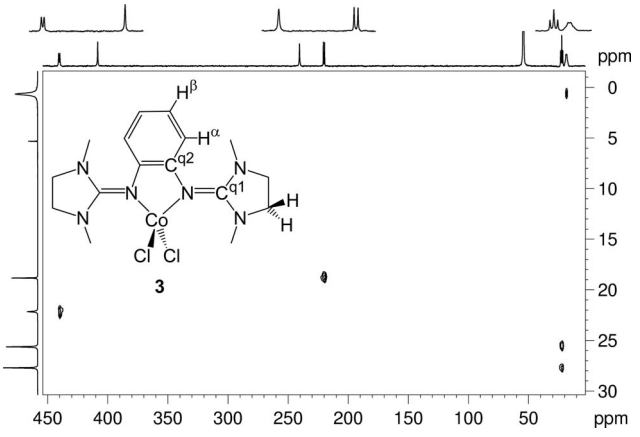

Figure 11. $^1J_{C,H}$ correlation NMR spectra of **3** (22 °C, direct detection, 600 MHz, CD_2Cl_2).

Table 3. Paramagnetic NMR spectroscopic shift data (150 MHz, CD_2Cl_2) and computed Fermi contact chemical shift at 295 K.

	CH$^\alpha$	CH$^\beta$	Me[a]	–CH$_2$–[a]	C^{q1}	C^{q2}
$\delta^{exptl.}_{HF,T}$ [ppm]	317.9	98.5	–17.9	–27.1	244.1	100.8
$\delta^{calcd.}_{con}$ [ppm]	323.1	80.4	–0.9	–8.5	170.0	–42.4

[a] Averaged values.

fects like dipolar interaction are small. However, the general trend is still in agreement. Thus, the resonance at δ = 407.6 ppm can be assigned to C^{q1} and the signal at δ = 239.9 ppm to C^{q2}. Although the calculated resonances for the $–CH_3$ and $–CH_2–$ groups also deviate from the observed one, it is possible to assign these signals unambiguously by 2D NMR spectroscopy as explained above.

Conclusion

Herein we have reported the structures and magnetic properties of a series of new Co^{II} and Ni^{II} complexes that feature chelating guanidine ligands. Mono- and dinuclear complexes were synthesized and analyzed. The results presented in this work provide a solid basis for future work in this field, which will especially focus on the redox properties of the complexes and the design of magnetic coordination polymers.

Experimental Section

General: All complexes were synthesized under argon by using standard Schlenk techniques. The solvents were dried with standard techniques. The bis(guanidine) ligand btmgb[4] as well as the tetrakis(guanidine) ligand ttmgb[17] were synthesized as described earlier. For the SQUID direct-current (dc) measurements, a Quantum Design MPMS-XL 5 was used. If not mentioned explicitly, all measurements were accomplished at an applied field of 500 G. IR and UV/Vis measurements were carried out with a BioRad Merlin Excalibur FT 3000 and a Perkin–Elmer Lambda 19 machine, respectively. NMR spectra were measured with a Bruker DRX 200, a Bruker Avance II 400, and a Bruker Avance III 600 spectrometer. The latter was equipped with a cryogenically cooled probe for direct detection of ^{13}C (QNPCryo Probe).

General Procedure for the Synthesis of the Ni^{II} Complexes (GP): The ligand (1 equiv.) was dissolved in dichloromethane and cooled to –80 °C. For the mononuclear complexes, an equimolar amount of the Ni^{II} salt was also dissolved in dichloromethane and cooled to –80 °C. For the dinuclear complexes, 2 equiv. of the Ni^{II} salt were employed. At this temperature, the ligand solution was added slowly to the suspension of the Ni^{II} salt, and the reaction mixture was slowly warmed to room temp. for 18 h. The reaction mixture was filtered off, and the solvent was removed in vacuo. The resulting solid was then washed three times with *n*-hexane to obtain the pure product.

Ligand bdmegb: 1,3-Dimethyl-2-imidazolidinone (2.7 mL, 25.00 mmol) was dissolved in absolute $CHCl_3$ (15 mL). Oxalyl chloride (10.9 mL, 125.00 mmol) was added dropwise to this solution. Afterwards, the solution was heated to 80 °C and then at reflux for 18 h. It was cooled to room temp., and the solvent was removed to obtain a brown-gold solid, which was washed two times with Et_2O (10 mL). The purified solid was directly dissolved in absolute CH_2Cl_2 (20 mL) and cooled to –10 °C. (1.08 g, 10.00 mmol). NEt_3 (6.3 mL, 45.00 mmol) was added, and this mixture was cooled to –10 °C as well. The solution of the activated urea was added slowly to this mixture, and the reaction was stirred at this temperature for 1 h. The reaction was quenched by the addition of 10% hydrochloric acid (25 mL). The reaction mixture was warmed to room temp., and the aqueous phase was extracted. The organic layer was washed another three times with 10% hydrochloride (20 mL) each. KOH solution (50%) was added to the combined aqueous phases until pH = 14 was reached. The product was extracted from the aqueous solution with toluene (4 × 25 mL), which was then dried with K_2CO_3, filtered off, and removed in vacuo to obtain colorless crystals (2.60 g, 8.65 mmol, 89%). $C_{16}H_{24}N_6$ (300.40): calcd. C 63.97, H 8.05, N 27.98; found C 63.87, H 8.01, N 27.90. ^1H NMR (400 MHz, $CDCl_3$): δ = 6.81 (m, 1 H, CH^{β}), 6.74 (m, 1 H, CH^{α}), 3.20 (s, 4 H, CH_2), 2.63 (s, 6 H, N-CH_3) ppm. ^{13}C NMR (100 MHz, $CDCl_3$): δ = 153.2 (CN_3), 142.1 ($C^{q,aromat}$), 122.7 (CH^{β}), 120.6 (CH^{α}), 48.5 (CH_2), 34.6 (NCH_3) ppm. IR (KBr): $\tilde{\nu}$ = 2931 (m), 2846 (s), 1659 (vs), 1573 (s), 1481 (s), 1435 (m), 1388 (s), 1280 (s), 1026 (s), 964 (m), 763 (m), 725 (m) cm^{-1}. HRMS (EI^+): *m*/*z* (%) = 300.2079 (100.00) $[M]^+$, 202.1342 (15.42) $[M – C_5H_{10}N_2]^+$, 188.1198 (29.69) $[M – C_5H_{10}N_3]^+$. Crystal data for $C_{16}H_{24}N_6$: M_r = 300.41, 0.35 × 0.30 × 0.30 mm, monoclinic, space group $P2_1/c$, a = 12.918(3) Å, b = 9.4990(19) Å, c = 14.527(3) Å, β = 111.83(3)°, V = 1654.8(6) $Å^3$, Z = 4, $d_{calcd.}$ = 1.206 $Mg\,m^{-3}$, θ_{range} = 1.70–30.00°. Reflections measd. 11180, indep. 4803, R_{int} = 0.0332. Final R indices [$I > 2\sigma(I)$]: R_1 = 0.0885, wR_2 = 0.1578.

Ligand btmgmpy: 2,6-Bis(hydroxymethyl)pyridine (5.00 g, 35.93 mmol) was dissolved in absolute $CHCl_3$ (60 mL) and cooled to 0 °C. Then PBr_3 (3.38 mL, 35.93 mmol) was added dropwise to the solution. The mixture was warmed to room temp., heated to 75 °C and then at reflux for 18 h. Subsequently, it was allowed to cool to room temp. before water (50 mL) was added. The organic layer was extracted, and the aqueous solution was washed three times with chloroform (40 mL portions). The organic layers were combined, washed with brine (40 mL), dried with $MgSO_4$, filtered, and the solvent was removed in vacuo to obtain colorless crystals (6.20 g, 23.40 mmol, 65%). ^1H NMR (200 MHz, $CDCl_3$): δ = 7.70 (t, ^3J = 7.6 Hz, 1 H, H^{para}), 7.37 (d, ^3J = 7.7 Hz, 2 H, H^{meta}), 4.53 (s, 4 H, CH_2) ppm.

2,6-Bis(bromomethyl)pyridine (3.00 g, 11.32 mmol) was combined in DMF (20 mL) with potassium phthalimide (4.19 g, 22.64 mmol) at room temp. and subsequently heated at reflux at 100 °C for 43 h. The reaction mixture was then allowed to cool to room temp., and crushed ice (50 mL) was added. It was kept for 2 h until precipitation was complete. The precipitate was filtered off, washed with water, and dried in vacuo for 48 h. Colorless 2,6-bis(phthalimidomethyl)pyridine (3.48 g, 8.77 mmol, 78%) was obtained. ^1H NMR (400 MHz, $CDCl_3$): δ = 7.76–7.66 (m, 8 H, H^{Phth}), 7.59 (t, ^3J = 7.7 Hz, 1 H, H^{para}), 7.12 (d, ^3J = 7.7 Hz, 2 H, H^{meta}), 4.91 (s, 4 H, CH_2) ppm.

2,6-Bis(phthalimidomethyl)pyridine (3.43 g, 8.62 mmol) was suspended in absolute EtOH (20 mL). An N_2H_4 solution (25.86 mL, 25.86 mmol; 1.0 M in thf) was added. The reaction mixture was then heated at reflux for 22 h (90 °C), allowed to cool to room temp., and by addition of 6 M HCl (20 mL) was brought to pH = 1. It was heated again to 100 °C for 2 h and subsequently kept overnight at room temp. until precipitation was completed. The precipitate was filtered off, washed with water, and the filtrate was then concentrated almost to dryness. A 50% KOH solution (5 mL) was added (up to pH = 14), and the aqueous layer extracted three times with chloroform (3 × 100 mL). The organic layers were combined, dried with $MgSO_4$, filtered, and the solvent was removed in vacuo to obtain 625.9 mg (4.56 mmol, 53%) of a white solid. ^1H NMR (400 MHz, $CDCl_3$): δ = 7.42 (t, ^3J = 7.7 Hz, 1 H, H^{para}), 6.96 (d, ^3J = 7.7 Hz, 2 H, H^{meta}), 3.77 (s, 4 H, CH_2), 1.57 (s, 4 H, NH_2) ppm. ^{13}C NMR (100 MHz, $CDCl_3$): δ = 161.03 (C^{quat}), 136.60 (C^{para}), 118.73 (C^{meta}), 47.37 (CH_2) ppm.

Tetramethylurea (1.21 mL, 10.05 mmol) was dissolved in absolute chloroform (8 mL). Oxalyl chloride (4.30 mL, 49.38 mmol) was

added dropwise, and the solution was heated at reflux at 80 °C for 18 h. The reaction mixture was allowed to cool to room temp., the solvent removed in vacuo, and the pale yellow precipitate washed three times with portions of diethyl ether (10 mL). The colorless guanidinium chloride was dried under vacuum. The diamine (600 mg, 4.37 mmol) was dissolved in absolute CH_2Cl_2 (20 mL), and dry triethylamine (2.62 mL, 18.79 mmol) was added. The guanidinium chloride was dissolved again in absolute CH_2Cl_2 (10 mL) and was subsequently added slowly to the diamine at –10 °C. The reaction mixture was stirred at –10 °C for 1 h, then 10% HCl (10 mL) was added, the phases were separated, and the organic layer was washed twice with 10% HCl (10 mL). The combined aqueous layers were washed with CH_2Cl_2 (10 mL), and then 50% KOH (20 mL) was added. The aqueous layer was extracted with toluene (3 × 20 mL). The combined toluene phases were dried with K_2CO_3, and the solvent was removed in vacuo to obtain a yellowish-white solid in 73% yield (1.03 g, 3.09 mmol). Crystals were grown from a solution in toluene at room temp. (m.p. 96.7 °C). $C_{17}H_{31}N_7$ (333.47): calcd. C 61.23, H 9.37, N 29.40; found C 61.27, H 9.38, N 28.96. ^{1}H NMR (400 MHz, $CDCl_3$): δ = 7.62 (t, ^3J = 7.6 Hz, 1 H, H^{para}), 7.48 (d, ^3J = 7.6 Hz, 2 H, H^{meta}), 4.51 (s, 4 H, CH_2), 2.77 (s, 12 H, NMe_2), 2.74 (s, 12 H, NMe_2) ppm. ^{13}C NMR (100 MHz, $CDCl_3$): δ = 162.32 (C^{Gua}), 161.06 (C^{ortho}), 136.67 (C^{para}), 118.33 (C^{meta}), 55.42 (CH_2), 39.63 (NMe_2), 38.91 (NMe_2) ppm. HRMS (EI$^+$): *m/z* (%) = 333.2630 (100.00) [M]$^+$, 218.1509 (29.05) [M – $C_5H_{13}N_3$]$^+$, 174.1033 (23.52) [M – $C_7H_{19}N_4$]$^+$, 160.0908 (22.21) [M – $C_8H_{21}N_4$]$^+$, 150.9996 (14.28) [M – $C_9H_{19}N_4$]$^+$, 132.0671 (20.12) [M – $C_9H_{23}N_5$]$^+$, 122.5821 (19.44) [M – $C_{11}H_{23}N_4$]$^+$, 106.0663 (25.84) [M – $C_{10}H_{23}N_6$]$^+$. IR (CsI): $\tilde{\nu}$ = 3001 (m), 2862 (m), 2808 (m), 1612 (m), 1504 (m) cm^{-1}. Crystal data for $C_{17}H_{31}N_7$: M_r = 333.49, 0.30 × 0.25 × 0.15 mm, monoclinic, space group $P2_1/c$, a = 15.327(3) Å, b = 8.2340(16) Å, c = 15.760(3) Å, β = 110.45(3)°, V = 1863.6(6) Å^3, Z = 4, $d_{calcd.}$ = 1.189 Mg m^{-3}, θ_{range} = 2.62–28.64°. Reflections measd. 9430, indep. 4774, R_{int} = 0.0536. Final R indices [$I > 2\sigma(I)$]: R_1 = 0.1054, wR_2 = 0.1386.

Complex 1: Ligand btmgb (130 mg, 0.43 mmol) was dissolved in acetonitrile (12 mL) at room temp.; $CoCl_2$ (54.7 mg, 0.42 mmol) was added to the yellow solution. After stirring the blue reaction mixture for 1 h, the solvent was removed in vacuo. The remaining solid was dissolved in CD_2Cl_2 (2 mL). After addition of *n*-hexane (5 mL), half of the solvent was removed in vacuo. The precipitating blue, crystalline solid of **1** was filtered off to yield 132.0 mg (0.28 mmol, 67%). The polycrystalline solid could be recrystallized from thf to obtain blue crystals of **1**·0.5thf, which could be analyzed by X-ray measurements. $C_{16}H_{28}Cl_2CoN_6$·0.5thf (470.33): calcd. C 45.97, H 6.86, N 17.87; found C 46.49, H 6.96, N 17.61. IR (KBr): $\tilde{\nu}$ = 3009 (w), 2942 (m), 2878 (m), 2793 (w), 1555 (vs), 1520 (vs), 1466 (vs), 1404 (vs), 1335 (m), 1180 (m), 1157 (m), 1033 (m), 818(m), 740 (vs), 563 (w) cm^{-1}. MS (FAB$^+$): *m/z* (%) = 433 (22) [M]$^+$, 400 (36) [M – Cl]$^+$, 399 (24) [M – Cl]$^+$, 398 (100) [M – Cl]$^+$, 305 (53) [btmgbH]$^+$. Crystal data for $C_{16}H_{28}Cl_2CoN_6$: M_r = 434.27, 0.35 × 0.25 × 0.25 mm, trigonal, space group $R\bar{3}$, a = 22.691(3) Å, b = 22.691(3) Å, c = 24.269(5) Å, V = 10822(3) Å^3, Z = 18, $d_{calcd.}$ = 1.199 Mg m^{-3}, θ_{range} = 1.79–28.68°. Reflections measd. 33980, indep. 6202, R_{int} = 0.0729. Final R indices [$I > 2\sigma(I)$]: R_1 = 0.0388, wR_2 = 0.0930.

Complex 2: Ligand btmgb (117.7 mg, 0.39 mmol) was added to a light purple suspension of $Co(OAc)_2$ (64.3 mg, 0.36 mmol) in ethanol (20 mL). After stirring the dark purple reaction mixture at room temp. for 1 h, the solvent was removed in vacuo. The remaining purple solid was dissolved in CH_2Cl_2 (2 mL). Then *n*-hexane (10 mL) was added and the solution half-concentrated in vacuo. The purple crystalline precipitate was filtered off to give **2** (44.3 mg, 0.09 mmol, 26%). The polycrystalline solid could be recrystallized from thf at –20 °C to obtain purple crystals suitable for X-ray diffraction measurements. $C_{20}H_{34}CoN_6O_4$ (481.45): calcd. C 49.89, H 7.12, N 17.46; found C 49.22, H 7.07, N 16.95. IR (KBr): $\tilde{\nu}$ = 3063 (w), 2924 (m), 2801 (w), 1520 (vs), 1397 (vs), 1327 (vs), 1157 (s), 1034 (s), 981 (m) 810 (m), 756 (m), 664 (s) cm^{-1}. MS (FAB$^+$): *m/z* (%) = 481 (3) [M]$^+$, 422 (100) [M – OAc]$^+$, 423 (26) [M – OAc]$^+$, 324 (3) [M – OAc]$^+$, 304 (19) [btmgb]$^+$, 305 (7) [btmgbH]$^+$. Crystal data for $C_{20}H_{34}CoN_6O_4$: M_r = 481.46, 0.35 × 0.30 × 0.30 mm, monoclinic, space group $P2_1/n$, a = 12.294(3) Å, b = 15.415(3) Å, c = 12.572(3) Å, β = 102.39(3)°, V = 2327.0(8) Å^3, Z = 4, $d_{calcd.}$ = 1.374 Mg m^{-3}, θ_{range} = 2.10–27.47°. Reflections measd. 10638, indep. 5317, R_{int} = 0.0284. Final R indices [$I > 2\sigma(I)$]: R_1 = 0.0361, wR_2 = 0.0928.

Complex 3: Ligand bdmegb (147.8 mg, 0.49 mmol) was dissolved in acetonitrile (15 mL) at room temp.; $CoCl_2$ (61.3 mg, 0.47 mmol) was added to this yellow solution. After stirring the blue reaction mixture for 1 h, the solvent was removed in vacuo. The remaining solid was dissolved in CH_2Cl_2 (2 mL). After addition of *n*-hexane (5 mL), half of the solvent was removed in vacuo. The precipitated blue, crystalline solid was filtered off to obtain **3** (153.1 mg, 0.36 mmol). This polycrystalline solid could be recrystallized from a solution in thf (around 22 mL) to obtain blue crystals that could be analyzed by X-ray measurements. $C_{16}H_{24}Cl_2CoN_6$ (430.24): calcd. C 44.67, H 5.62, N 19.53; found C 43.40, H 5.62, N 18.89. IR (KBr): $\tilde{\nu}$ = 3048 (w), 2940 (w), 2878 (w), 2801 (w), 1589 (vs), 1551 (vs), 1481 (vs), 1412 (vs), 1389 (s), 1288 (s), 1234 (m), 1034 (m), 980 (w), 887 (w), 818 (m), 764 (m), 741 (m) cm^{-1}. HRMS (FAB$^+$): *m/z* (%) = 429.0768 (39.65) [M]$^+$, 394.1098 (100) [M – Cl]$^+$, 364.2863 (10.91) [M – ClC_2H_6]$^+$, 300.2048 (27.94) [bdmegb]$^+$. Crystal data for $C_{16}H_{24}Cl_2CoN_6$: M_r = 430.24, 0.35 × 0.30 × 0.30 mm, monoclinic, space group $P2_1/c$, a = 12.062(2) Å, b = 10.001(2) Å, c = 15.991(3) Å, β = 93.35(3)°, V = 1925.7(7) Å^3, Z = 4, $d_{calcd.}$ = 1.484 Mg m^{-3}, θ_{range} = 1.69–33.14°. Reflections measd. 7338, indep. 7338, R_{int} = 0.0238. Final R indices [$I > 2\sigma(I)$]: R_1 = 0.0284, wR_2 = 0.0768.

Complex 4a: The complex was synthesized according to the GP by using bdmegb (224.5 mg, 0.75 mmol), $NiCl_2$–dme adduct (164.2 mg, 0.75 mmol), and CH_2Cl_2 (2 × 5 mL). A green solid (64.5 mg, 0.65 mmol, 87%) was obtained. Crystals suitable for X-ray measurements were grown from CH_2Cl_2 and *n*-hexane. $C_{16}H_{24}Cl_2N_6Ni$ (430.00): calcd. C 44.69, H 5.63, N 19.54; found C 44.98, H 5.60, N 19.13. IR (KBr): $\tilde{\nu}$ = 2932 (m), 2870 (m), 1597 (s), 1558 (vs), 1481 (s), 1411 (s), 1288 (s), 1242 (m), 1033 (m), 763 (m) cm^{-1}. UV/Vis (CH_2Cl_2): λ (ε, L mol^{-1} cm^{-1}) = 290 (13930), 314 (10277), 445 (587), 511 (289), 587 (195), 693 (99) nm. HRMS (EI$^+$): *m/z* (%) = 430.0784 (35.58) [M]$^+$, 393.1085 (16.92) [M – Cl]$^+$, 300.2034 (100.00) [bdmegb]$^+$, 299.1946 (100.00) [bdmegb-H]$^+$. Crystal data for $C_{16}H_{24}Cl_2N_6Ni$: M_r = 430.02, 0.40 × 0.35 × 0.35 mm, monoclinic, space group $P2_1/n$, a = 12.666(3) Å, b = 11.299(2) Å, c = 14.104(3) Å, β = 108.71(3)°, V = 1911.8(7) Å^3, Z = 4, $d_{calcd.}$ = 1.494 Mg m^{-3}, θ_{range} = 1.88–29.13°. Reflections measd. 5158, indep. 5158, R_{int} = 0.0382. Final R indices [$I > 2\sigma(I)$]: R_1 = 0.0377, wR_2 = 0.0938.

Complex 4b: The complex was synthesized according to the GP by using bdmegb (247.1 mg, 0.83 mmol), $NiBr_2$–dme adduct (253.9 mg, 0.83 mmol), and CH_2Cl_2 (2 × 5 mL). After workup, a brown solid was obtained in 91% yield (390.7 mg, 0.75 mmol). $C_{16}H_{24}Br_2N_6Ni$ (518.90): calcd. C 37.03, H 4.66, N 16.20; found C 37.53, H 4.78, N 16.05. IR (KBr): $\tilde{\nu}$ = 2932 (m), 2870 (m), 1597 (s), 1558 (vs), 1481 (s), 1411 (s), 1288 (s), 1234 (m), 1033 (m), 763

(m) cm^{-1}. UV/Vis (CH_2Cl_2): λ (ε, $L\,mol^{-1}\,cm^{-1}$) = 251 (17800), 292 (11673), 473 (665), 536 (473), 605 (283), 721 (100) nm. HRMS (EI^+): *m/z* (%) = 517.9731 (100.00) $[M]^+$, 437.0536 (37.79) $[M - Br]^+$.

Complex 5a: The complex was synthesized in modification to the GP by using btmgmpy (200.1 mg, 0.60 mmol, 1.2 equiv.), $NiCl_2$–dme adduct (109.9 mg, 0.50 mmol), and CH_2Cl_2 (2 × 10 mL). The crude product was washed three times with toluene (2 mL) to obtain a green-yellow precipitate in 87% yield (201.9 mg, 0.44 mmol). Crystals suitable for X-ray diffraction measurements were obtained in a CH_2Cl_2/*n*-hexane mixture. $C_{17}H_{31}Cl_2N_7Ni$ (463.07): calcd. C 44.09, H 6.75, N 21.17; found C 44.24, H 6.84, N 20.93. IR (CsI): $\tilde{\nu}$ = 3001 (w), 2931 (m), 2877 (m), 2800 (w), 1573 (s), 1527 (s), 1465 (s), 1427 (s), 1396 (s), 1335 (m), 1249 (s), 1149 (vs), 1072 (s), 1033 (s), 910 (s), 810 (vs), 771 (m), 740 (m), 586 (m) cm^{-1}. UV/Vis (CH_2Cl_2): λ (ε, $L\,mol^{-1}\,cm^{-1}$) = 316 (11172), 523 (163) nm. HRMS (EI^+): *m/z* (%) = 463.1315 (3.29) $[M]^+$, 425.1084 (100.00) $[M - HCl]^+$, 333.2652 (25.44) $[btmgmpy]^+$. Crystal data for (**5a**)$_2$·CH_2Cl_2, $C_{35}H_{64}Cl_6N_{14}Ni_2$: M_r = 1011.08, 0.40 × 0.40 × 0.40 mm, monoclinic, space group $P2_1/n$, a = 8.9850(18) Å, b = 15.382(3) Å, c = 17.460(4) Å, β = 104.05(3)°, V = 2340.9(8) Å^3, Z = 2, $d_{calcd.}$ = 1.432 $Mg\,m^{-3}$, θ_{range} = 1.79–33.00°. Reflections measd. 18757, indep. 8823, R_{int} = 0.0544. Final R indices [$I > 2\sigma(I)$]: R_1 = 0.0478, wR_2 = 0.1255.

Complex 5b: The complex was synthesized according to the GP by using btmgmpy (166.8 mg, 0.50 mmol), $NiBr_2$–dme adduct (154.3 mg, 0.50 mmol), and CH_2Cl_2 (2 × 15 mL). A green solid was obtained in 88% yield (241.7 mg, 0.44 mmol). $C_{17}H_{31}Br_2N_7Ni$ (551.98): calcd. C 36.99, H 5.66, N 17.76; found C 36.83, H 5.94, N 17.36. IR (CsI): $\tilde{\nu}$ = 3001 (w), 2931 (m), 2877 (m), 2793 (w), 1566 (s), 1527 (s), 1465 (s), 1396 (s), 1334 (m), 1257 (s), 1157 (vs), 1064 (s), 1033 (s), 910 (s), 802 (vs), 771 (m), 586 (m) cm^{-1}. UV/Vis (CH_2Cl_2): λ (ε, $L\,mol^{-1}\,cm^{-1}$) = 324 (6757), 534 (199) nm. HRMS (EI^+): *m/z* (%) = 472.1140 (100.00) $[M - Br]^+$, 426.1678 (11.46) $[M - NC_2H_6Br]^+$, 390.1888 (47.83) $[M - Br_2]^+$, 333.2609 (9.89) $[btmgmpy]^+$.

Complex 6: A blue solution of $CoCl_2$ (65.6 mg, 0.50 mmol) in CH_3CN (6 mL) at 60 °C was added to a solution of ttmgb (111.0 mg, 0.20 mmol) in CH_3CN (8 mL). The resulting green reaction mixture was stirred at 70 °C for 30 min. Then the solvent was removed, and the resulting green solid was dissolved in CH_2Cl_2 (16 mL). The solution was filtered off and overlaid with *n*-hexane (8 mL) to obtain small green crystals at –20 °C after 48 h. Yield: 80.4 mg (0.09 mmol, 46%). $C_{26}H_{50}Cl_4Co_2N_{12}$ (790.43): calcd. C 40.45, H 6.42, N 21.90; found C 39.64, H 6.65, N 21.63. IR (CsI): $\tilde{\nu}$ = 3009 (w), 2943 (m), 2878 (w), 2797 (w), 1555 (vs), 1520 (vs), 1485 (s), 1481 (vs), 1331 (m), 1180 (m), 1157 (m), 1030 (m), 891 (m), 814, (m) 718 (m) cm^{-1}. MS (FAB^+): *m/z* (%) = 659 (8) $[M - CoCl_2]^+$, 531 (52) $[ttmgbH]^+$, 486 (27) $[ttmgb - N(CH_3)_2]^+$.

Complex 7: Ligand ttmgb (180.1 mg, 0.34 mmol) was added to a light purple suspension of $Co(OAc)_2$ (117.1 mg, 0.66 mmol) in ethanol (14 mL). After stirring the red-brown reaction mixture at room temp. for 1 h, the solvent was removed in vacuo. The remaining brown solid was recrystallized from a solution in thf (24 mL). Complex **7** (227.1 mg, 0.26 mmol, 78%) was thus obtained. These crystals appeared red or yellow-green depending on the angle of view, and could be analyzed by XRD measurements. $C_{34}H_{62}Co_2N_{12}O_8$ (884.80): calcd. C 46.15, H 7.06, N 19.00; found C 45.36, H 7.22, N 18.29. IR (KBr): $\tilde{\nu}$ = 2986 (w), 2924 (s), 2870 (m), 2793 (w), 1520 (vs), 1466 (vs), 1397 (vs), 1327 (s), 1281 (m), 1150 (s), 1026 (s), 845 (m), 802 (m), 671 (s) cm^{-1}. MS (FAB^+): *m/z* (%) = 649 (100) $[Co_2(ttmgb)H]^+$, 531 (52) $[ttmgbH]^+$, 487 (30) $[ttmgb–N(CH_3)_2]^+$, 305 (31) $[ttmgbH–2NC(NMe_2)_2]^+$. Crystal data for **7**·0.9C_4H_8O, $C_{37.60}H_{69.20}Co_2N_{12}O_{8.90}$: M_r = 949.71, 0.40 × 0.35 × 0.30 mm, triclinic, space group $P\bar{1}$, a = 17.070(3) Å, b = 17.719(4) Å, c = 17.898(4) Å, α = 67.09(3)°, β = 89.20(3)°, γ = 84.61(3)°. V = 4962.9(17) Å^3, Z = 8, $d_{calcd.}$ = 1.271 $Mg\,m^{-3}$, θ_{range} = 1.20–27.48°. Reflections measd. 42523, indep. 22702, R_{int} = 0.0339. Final R indices [$I > 2\sigma(I)$]: R_1 = 0.0514, wR_2 = 0.1455.

Complex 8a: By applying the GP, the complex was synthesized by using ttmgb (132.6 mg, 0.25 mmol), $NiCl_2$–dme adduct (109.9 mg, 0.5 mmol), and CH_2Cl_2 (2 × 15 mL). A brown solid was obtained as product. Yield: 92% (182.1 mg, 0.23 mmol). Crystals suitable for XRD could be obtained at room temp. in CH_2Cl_2 under an *n*-hexane layer. $C_{26}H_{50}Cl_4N_{12}Ni_2$ (789.95): calcd. C 39.53, H 6.38, N 21.28; found C 40.94, H 7.28, N 21.53. IR (CsI): $\tilde{\nu}$ = 2936 (w), 1628 (m), 1524 (m), 1404 (m), 1315 (m), 1177 (m), 1034 (m), 895 (w), 814 (w) cm^{-1}. UV/Vis (CH_2Cl_2): λ (ε, $L\,mol^{-1}\,cm^{-1}$) = 283 (31607), 338 (22269), 456 (678), 493 (620), 533 (58) nm. HRMS (EI^+): *m/z* (%) = 788.1658 (20.36) $[M]^+$, 660.2958 (100.00) $[M - NiCl_2]^+$. Crystal data for **8a**·2CH_2Cl_2, $C_{28}H_{54}Cl_8N_{12}Ni_2$: M_r = 859.81, 0.30 × 0.15 × 0.15 mm, monoclinic, space group $P2_1/n$, a = 13.908(3) Å, b = 11.188(2) Å, c = 15.572(3) Å, β = 114.51(3)°, V = 2204.7(8) Å^3, Z = 2, $d_{calcd.}$ = 1.446 $Mg\,m^{-3}$, θ_{range} = 1.65–33.00°. Reflections measd. 19231, indep. 8306, R_{int} = 0.0340. Final R indices [$I > 2\sigma(I)$]: R_1 = 0.0396, wR_2 = 0.1043.

Complex 8b: By applying the GP, the complex was synthesized by using ttmgb (132.6 mg, 0.25 mmol), $NiBr_2$–dme adduct (154.3 mg, 0.50 mmol), and CH_2Cl_2 (2 × 15 mL), which yielded a purple solid (184.2 mg, 0.19 mmol, 76%). $C_{26}H_{50}Br_4N_{12}Ni_2$ (967.76): calcd. C 32.27, H 5.21, N 17.37; found C 33.13, H 6.08, N 17.30. IR (CsI): $\tilde{\nu}$ = 2936 (w), 1628 (m), 1562 (m), 1400 (s), 1331 (m), 1157 (m), 1030 (m), 895 (w), 814 (w) cm^{-1}. UV/Vis (CH_2Cl_2): λ (ε, $L\,mol^{-1}\,cm^{-1}$) = 280 (38667), 335 (27978), 532(890), 616 (590) nm. HRMS (EI^+): *m/z* (%) = 965.9666 (45.28) $[M]^+$, 887.0544 (3.46) $[M - Br]^+$, 750.1630 (100.00) $[M - NiBr_2]^+$.

Complex 9: The GP was applied by using ttmgb (262.2 mg, 0.50 mmol), $Ni(acac)_2$ (256.9 mg, 1.00 mmol), and CH_2Cl_2 (2 × 15 mL). A green solid was obtained in 67% yield (351.0 mg, 0.34 mmol). Crystals suitable for XRD could be obtained at room temp. in CH_2Cl_2 and *n*-hexane. $C_{46}H_{78}N_{12}Ni_2O_8$ (1044.57): calcd. C 52.89, H 7.53, N 16.09; found C 50.98, H 7.42, N 15.45. IR (CsI): $\tilde{\nu}$ = 2920 (m), 1616 (s), 1512 (s), 1474 (s), 1420 (s), 1254 (m), 1188 (m), 1150 (m), 1026 (m), 918 (m), 748 (m), 710 (m) cm^{-1}. UV/Vis (CH_2Cl_2): λ (ε, $L\,mol^{-1}\,cm^{-1}$) = 245 (13871), 302 (20332), 356 (7135), 400 (7393), 632 (644) nm. MS (FAB^+): *m/z* (%) = 1042.6 (10) $[M]^+$, 786.5 (40) $[M - Ni(acac)_2]$, 687.5 (100) $[M - acac–Ni(acac)_2]$, 530.5 (100) $[ligand]^+$. HRMS (FAB^+): *m/z* (%) = 1042.4756 (100.00) $[M]^+$, 943.4452 (21.93) $[M - acac]^+$. Crystal data for 2(**9**·3.5CH_2Cl_2) $C_{99}H_{170}Cl_{14}N_{24}Ni_4O_{16}$: M_r = 2683.65, 0.40 × 0.35 × 0.35 mm, monoclinic, space group $P2_1/c$, a = 12.818(3) Å, b = 12.583(3) Å, c = 21.923(4) Å, β = 106.97(3)°, V = 3382.0(12) Å^3, Z = 1, $d_{calcd.}$ = 1.318 $Mg\,m^{-3}$, θ_{range} = 1.89–30.02°. Reflections measd. 30582, indep. 9601, R_{int} = 0.0556. Final R indices [$I > 2\sigma(I)$]: R_1 = 0.0583, wR_2 = 0.1472.

X-ray Crystallographic Studies: Suitable crystals were taken directly out of the mother liquor, immersed in perfluorinated polyether oil, and fixed on top of a glass capillary. Measurements were made with a Nonius-Kappa CCD diffractometer with a low-temperature unit by using graphite-monochromated Mo-K_α radiation. The temperature was set to 100 K. The data collected were processed with the standard Nonius software.[30] All calculations were performed with the SHELXT-PLUS software package. Structures were solved by direct methods with the SHELXS-97 program and refined with

the SHELXL-97 program.[31,32] Graphical handling of the structural data during solution and refinement was performed with XPMA.[33] Atomic coordinates and anisotropic thermal parameters of non-hydrogen atoms were refined by full-matrix least-squares calculations. CCDC-769728 (btmgmpy), -769730 (bdmegb), -769724 (**1**), -769726 (**2**), -769727 (**3**), -769731 (**4a**), -769729 (**5a**), -769725 (**7**), -769723 (**8a**), and -770193 (**9**) contain the supplementary crystallographic data for this paper. These data can be obtained free of charge from The Cambridge Crystallographic Data Centre via www.ccdc.cam.ac.uk/data_request/cif.

Computational Details: Quantum chemical calculations were carried out in the framework of density functional theory. The calculations relied on the program package TURBOMOLE.[34,35] The BP86[36,37] and B3LYP[38–40] functionals were used in combination with the def2-SV(P)[41] basis set. The calculations with the BP86 functional made use of the RI approximation for the two-electron integrals.[42] The appropriate auxiliary basis sets were employed.[43] For the numerical integration the grid "m4" was applied. SCF energies were converged to 1×10^{-7} hartree. During the structure optimizations the maximum gradient was converged to 1×10^{-4} hartree bohr^{-1}.

Supporting Information (see also the footnote on the first page of this article): Illustration of the structures of the bdmegb and the btmgmpy ligands as well as the salt $[(bdmegb)H_2][NiCl_4]$, statistics of the Cl–Ni–Cl angle in tetrahedral Ni^{II} complexes with chelating nitrogen ligands, calculated structures of the *cis* and *trans* isomers of the complex $[(btmgb)CoCl_2]$, and visualization of the molecular structure of **4b**.

Acknowledgments

The authors gratefully acknowledge continuous financial support by the DFG (Deutsche Forschungsgemeinschaft) especially through the Graduate College 850 and the priority program SPP 1178.

[1] See, for example: F. T. Edelmann, *Adv. Organomet. Chem.* **2008**, *57*, 183–352.
[2] S. Herres-Pawlis, *Nachr. Chem.* **2009**, *57*, 20–23.
[3] See, for example: S. Herres-Pawlis, A. Neuba, O. Seewald, T. Seshadri, H. Egold, U. Flörke, G. Henkel, *Eur. J. Org. Chem.* **2005**, 4879–4890.
[4] M. Kawahata, K. Yamaguchi, T. Ho, T. Ishikawa, *Acta Crystallogr., Sect. E: Struct. Rep. Online* **2006**, *62*, o3301–o3302.
[5] A. Peters, U. Wild, O. Hübner, E. Kaifer, H.-J. Himmel, *Chem. Eur. J.* **2008**, *14*, 7813–7821.
[6] M. Reinmuth, U. Wild, E. Kaifer, M. Enders, H. Wadepohl, H.-J. Himmel, *Eur. J. Inorg. Chem.* **2009**, 4795–4808.
[7] P. Roquette, A. Maronna, A. Peters, E. Kaifer, H.-J. Himmel, C. Hauf, V. Herz, E.-W. Scheidt, W. Scherer, *Chem. Eur. J.* **2010**, *16*, 1336–1350.
[8] V. Raab, J. Kipke, R. M. Gschwind, J. Sundermeyer, *Chem. Eur. J.* **2002**, *8*, 1682–1693.
[9] U. Wild, O. Hübner, A. Maronna, M. Enders, E. Kaifer, H. Wadepohl, H.-J. Himmel, *Eur. J. Inorg. Chem.* **2008**, 4440–4447.
[10] J. Börner, S. Herres-Pawlis, U. Flörke, K. Huber, *Eur. J. Inorg. Chem.* **2007**, 5645–5651.
[11] A. Neuba, R. Hasse, M. Bernard, U. Floeke, S. Herres-Pawlis, *Z. Anorg. Allg. Chem.* **2008**, *634*, 2511–2517.
[12] D. Petrovic, T. Glöge, T. Bannenberg, C. G. Hrib, S. Randoll, P. G. Jones, M. Tamm, *Eur. J. Inorg. Chem.* **2007**, 3472–3475.
[13] D. Petrovic, T. Bannenberg, S. Randoll, P. G. Jones, M. Tamm, *Dalton Trans.* **2007**, 2812–2822.
[14] J. Börner, U. Flörke, T. Glöge, T. Bannenberg, M. Tamm, M. D. Jones, A. Döring, D. Kuckling, S. Herres-Pawlis, *J. Mol. Catal. A* **2010**, *316*, 139–145.
[15] T. Isobe, K. Fukuda, T. Ishikawa, *J. Org. Chem.* **2000**, *65*, 7770–7773.
[16] H. Wittmann, Dissertation, **1999**, Philipps-University Marburg.
[17] A. Peters, E. Kaifer, H.-J. Himmel, *Eur. J. Org. Chem.* **2008**, 5907–5914.
[18] V. Vitske, C. König, O. Hübner, E. Kaifer, H.-J. Himmel, *Eur. J. Inorg. Chem.* **2010**, 115–126.
[19] C. Trumm, O. Hübner, E. Kaifer, H.-J. Himmel, *Eur. J. Inorg. Chem.* **2010**, 3102–3108.
[20] A. Peters, C. Trumm, M. Reinmuth, D. Emeljanenko, E. Kaifer, H.-J. Himmel, *Eur. J. Inorg. Chem.* **2009**, 3791–3800.
[21] In modification of the following: H. Scheytza, O. Rademacher, H.-U. Reißig, *Eur. J. Org. Chem.* **1999**, 2373–2381.
[22] In modification of the following: D. Chen, A. E. Martell, Y. Sun, *Inorg. Chem.* **1989**, *28*, 2647–2652.
[23] The Cambridge Structural Database: a quarter of a million crystal structures and rising: F. H. Allen, *Acta Crystallogr., Sect. B* **2002**, *58*, 380 388.
[24] R. Bauernschmitt, R. Ahlrichs, *Chem. Phys. Lett.* **1996**, *256*, 454–464.
[25] a) D. F. Evans, *J. Chem. Soc.* **1959**, 2003–2005; b) D. F. Evans, G. V. Fazakerley, R. F. Phillips, *J. Chem. Soc. A* **1971**, 1931–1934; c) J. Löliger, R. Schefflod, *J. Chem. Educ.* **1972**, *49*, 646–647; d) D. H. Grant, *J. Chem. Educ.* **1995**, *72*, 39–40; e) C. Piguet, *J. Chem. Educ.* **1997**, *74*, 815–816.
[26] For an instructive derivation, see: a) R. Boča, *Theoretical Foundations of Molecular Magnetism*, Lausanne, Elsevier Science S. A., Lausanne, **1999**; b) R. Boča, *Coord. Chem. Rev.* **2004**, *248*, 757 815.
[27] Program julX written by E. Bill: http://ewww.mpi-muelheim.mpg.de/bac/logins/bill/julX_en.php.
[28] P. Roquette, A. Maronna, M. Reinmuth, M. Enders, H.-J. Himmel, *J. Am. Chem. Soc.*, submitted for publication.
[29] P. Fernández, H. Pritzkow, J. Carbó, P. Hofmann, M. Enders, *Organometallics* **2007**, *26*, 4402–4412.
[30] *DENZO-SMN, Data Processing Software*, Nonius **1998**, ttp://www.nonius.com.
[31] a) G. M. Sheldrick, *SHELXS-97*, *Program for Crystal Structure Solution*, University of Göttingen, **1997**, http://shelx.uni-ac.gwdg.de/SHELX/index.html; b) G. M. Sheldrick, *SHELXL-97*, *Program for Crystal Structure Refinement*, University of Göttingen, **1997**, http://shelx.uni-ac.gwdg.de/SHELX/index.html.
[32] *International Tables for X-ray Crystallography*, Kynoch Press, Birmingham, U.K., **1974**, vol. 4.
[33] L. Zsolnai, G. Huttner, *XPMA*, University of Heidelberg, **1994**, http://www.uni-heidelberg.de/institute/fak12/AC/huttner/software/software.html.
[34] R. Ahlrichs, M. Bär, M. Häser, H. Horn, C. Kölmel, *Chem. Phys. Lett.* **1989**, *162*, 165–169.
[35] O. Treutler, R. Ahlrichs, *J. Chem. Phys.* **1995**, *102*, 346–354.
[36] A. D. Becke, *Phys. Rev. A* **1988**, *38*, 3098–3100.
[37] J. P. Perdew, *Phys. Rev. B* **1986**, *33*, 8822–8824.
[38] P. J. Stephens, F. J. Devlin, C. F. Chabalowski, M. J. Frisch, *J. Phys. Chem.* **1994**, *98*, 11623–11627.
[39] A. D. Becke, *J. Chem. Phys.* **1993**, *98*, 5648–5652.
[40] C. Lee, W. Yang, R. G. Parr, *Phys. Rev. B* **1988**, *37*, 785–789.
[41] F. Weigend, R. Ahlrichs, *Phys. Chem. Chem. Phys.* **2005**, *7*, 3297–3305.
[42] K. Eichkorn, O. Treutler, H. Öhm, M. Häser, R. Ahlrichs, *Chem. Phys. Lett.* **1995**, *242*, 652–660.
[43] F. Weigend, *Phys. Chem. Chem. Phys.* **2006**, *8*, 1057–1065.

Received: March 18, 2010
Published Online: August 24, 2010

